JOURNAL OF Materials CHEMISTRY

Temperature-controlled growth of α-Al_2O_3 nanobelts and nanosheets

X. S. Fang,* C. H. Ye, X. S. Peng, Y. H. Wang, Y. C. Wu and L. D. Zhang

Laboratory of Functional Nanomaterials and Nanostructures, Institute of Solid State Physics, Chinese Academy of Sciences, P. O. Box 1129, Hefei 230031, P. R. China.
E-mail: xshfang@yahoo.com.cn; Fax: +86-551-5591434

Received 29th August 2003, Accepted 8th October 2003
First published as an Advance Article on the web 29th October 2003

α-Al_2O_3 Nanobelts and nanosheets with different morphologies and sizes have been successfully synthesized by a simple chemical route from H_2O and Al in an argon atmosphere. Scanning electron microscopy (SEM) and transmission electron microscopy (TEM) observations show that the as-synthesized α-Al_2O_3 nanostructures consist of nanobelts and nanosheets. We find that the temperature distribution inside the alumina tube is the critical factor determining the morphologies and sizes of the α-Al_2O_3 nanostructures. Photoluminescence measurements showed a blue luminescence band in the wavelength range of 400–500 nm, which can be attributed to F^+ centers in the α-Al_2O_3 nanostructures. The growth of these products is believed to be mainly determined by growth kinetics as well as thermodynamics.

1. Introduction

One-dimensional nanostructures have received much attention due to their potential interest for understanding fundamental physical concepts and for applications in constructing nanoscale electric and optoelectronic devices.[1] Up to now, much attention has been paid to the preparation of nanostructures of the family of oxides with interesting optical and electrical properties. Several binary oxide nanostructures such as Ga_2O_3, GeO_2, In_2O_3, SiO_2 and ZnO have been successfully synthesized.[2–8]

Owing to their brittleness, ceramics have been regarded as materials of modest performance, especially under tension or bending conditions, In contrast to metals or polymers, however, the thermal stability of ceramics above 700 °C makes them suitable materials for high-temperature applications. Microstructural design is critical in order to obtain reliable ceramic materials. Such materials are usually called "advanced ceramics".[9] Recently, an enormous effort has been paid to obtain alumina and aluminosilicate fibers with a high Al_2O_3 content. For example, Al_2O_3 nanowires and nanobelts have recently been synthesized through an *in-situ* catalytic growth and thermal evaporation.[10,11]

In previous work, it was proposed that the growth of nanostructures with different morphologies, sizes, compositions and microstructures was mainly controlled by the temperature and duration of the reaction process.[12–16] In this article, we systematically investigate the α-Al_2O_3 nanostructures produced from a simple chemical route as a function of the local temperature. Our results show that the temperature distribution inside the alumina tube is the critical factor for the morphologies and sizes of the α-Al_2O_3 nanostructures.

2. Experimental

Ultrahigh purity (99.999%) aluminium was placed at a ceramic boat. Then, this boat was inserted at the center of the horizontal alumina tube furnace for heating. A long alumina plate (6 cm in length and 16 mm in width) was placed to act as the deposition substrate. Water was introduced into the reaction by placing an alumina crucible containing about 50 ml distilled water in the upstream side of the alumina tube.

The system was rapidly heated to 1350 °C in 12 min and kept at this temperature for 2 h in a flowing atmosphere with Ar both as protecting medium and as carrying gas. During the heating process, the Ar flow rate was kept at 50 sccm (standard $cm^3\ min^{-1}$). After the system was cooled to room temperature, four distinct zones of white, wool-like products were formed along the whole alumina plate.

The as-synthesized products were characterized and analyzed by scanning electron microscopy [(SEM) JEOL JSM 6700F], X-ray diffraction [(XRD) PW1710 instrument with Cu-Kα radiation], and transmission electron microscopy [(TEM) JEOL 2010, operated at 200 kV]. For SEM observations, the product was pasted on an Al substrate using conductive carbon paste. Specimens for TEM investigations were briefly ultra-sonicated in ethanol, and then a drop of the suspension was placed on a carbon film coated holey copper grid. The photoluminescence (PL) spectrum was obtained using an Edinburgh FLS 920 fluorescence spectrophotometer (Xe 900 lamp) at room temperature. The excitation wavelength was 255 nm and the filter wavelength was 310 nm.

3. Results and discussion

Four distinct zones can be roughly defined through the deposition thickness of the as-synthesized products. With an increase in temperature from 1100 to 1300 °C, the thicknesses decrease gradually from about 2 mm to 50 μm. Further investigations showed that the first two zones consisted of α-Al_2O_3 nanobelts with typical widths ranging from 10 to 500 nm, however, the other two zones consisted of α-Al_2O_3 nanosheets with typical widths varying from 1 to 10 μm. On the basis of the appearances described above and the curve diagram of temperature and deposition distance, four distinctive temperature zones were identified: zone I (1100–1150 °C), zone II (1150–1200 °C), zone III (1200–1250 °C) and zone IV (1250–1300 °C). Fig. 1(a) schematically depicts the position of the four zones inside the alumina tube. The corresponding diagram of temperature and deposition distance is shown in Fig. 1(b).

3.1. Zone I (1100–1150 °C)

Products (the thickest deposition layer, about 2 mm) were formed in zone I. The length of this zone is about 21 mm. The morphology of the products was examined using SEM. A

 DOI: 10.1039/b309193g

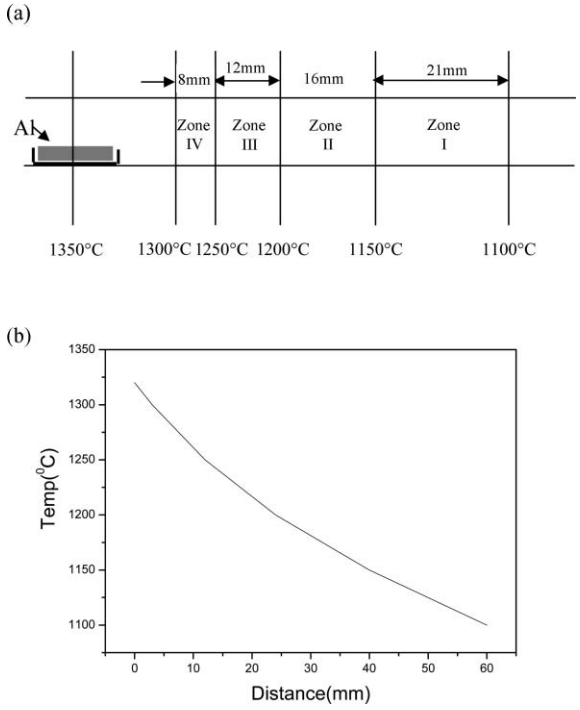

Fig. 1 (a) Schematic diagram of the four distinctive growth zones inside the alumina tube. The deposition widths and temperature ranges of these zones are also shown. (b) Diagram of temperature and deposition distance.

typical SEM image (Fig. 2(a)) shows that large-scale Al_2O_3 nanobelts were formed in high yield with widths varying from 10 to 100 nm. A representative SEM of a single nanobelt (Fig. 2(b)) reveals that the nanobelt has a thickness of 10 nm and width of 50 nm. The nanobelt has a prefect morphology, as can be seen from its sharp edges.

Further structural characterization was carried out using TEM. Fig. 2(c) shows an individual Al_2O_3 nanobelt, which was further characterized by selected area electron diffraction (SAED) and HRTEM, as illustrated in Fig. 2(d). The corresponding lattice-resolved TEM image and SAED pattern (inset) recorded perpendicular to the axis of this nanobelt, revealed that the Al_2O_3 nanobelt is single-crystalline with an inter-plane spacing of 0.428 nm, in agreement with the *d* value of the (003) planes of α-Al_2O_3 crystals (d = 0.433 nm) with growth along the <001> direction.[17]

3.2. Zone II (1150–1200 °C)

With the increase of the substrate temperature, the deposition thickness decreases, and the width of the Al_2O_3 nanobelts increases. The deposition thickness of the products formed in zone II is about 400 μm and the length of this zone is about 16 mm. The SEM images of these nanostructures formed in this zone (Fig. 3(a)) are belt-like, which is distinct in shape from known nanotubes and nanowires. In addition, many twisted and curved belt-like nanostructures are also observed, which suggests that the nanobelts might be flexible or might be not as brittle as bulk alumina. Most nanobelts have uniform widths along entire lengths with sharp and regular edges, and the typical widths of the nanobelts vary from 100 to 500 nm.

3.3. Zone III (1200–1250 °C)

Products (a comparatively thin deposition layer, about 100 μm) were formed in zone III. The length of this zone is about 12 mm. A common feature of inorganic fiber growth is the presence of various slightly different crystals arising from the same procedure,[9,18] due to different mechanisms occurring simultaneously or to same deposition mechanism taking place

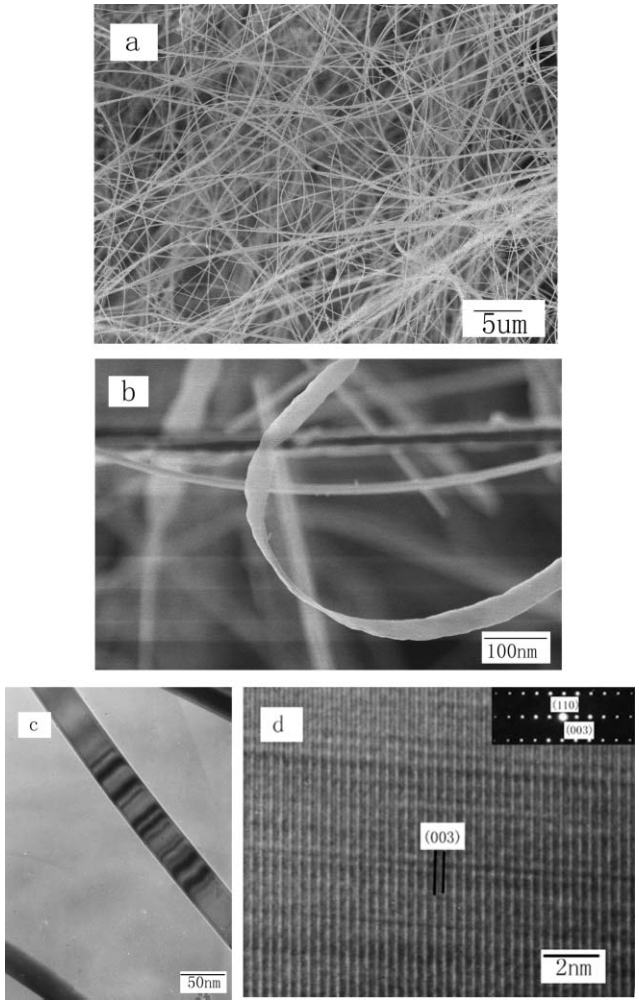

Fig. 2 The structure of Al_2O_3 nanobelts formed in zone I: (a) SEM image of the as-synthesized large-scale Al_2O_3 nanobelts with widths varying from 10 to 100 nm. (b) Representative SEM of a single nanobelt with a thickness of 10 nm and width of 50 nm. (c) TEM image of an individual Al_2O_3 nanobelt. (d) HRTEM image of an Al_2O_3 nanobelt and SAED pattern (inset) of the nanobelt.

at distinct furnace zones. Here, a novel type of Al_2O_3 nanosheets, unlike the hexagonal fibers, having two parallel flat faces and very small thickness, are shown in Fig. 3(b). The typical widths of these nanosheets are approximately 1–5 μm and the thickness is in the range of 10–50 nm.

3.4. Zone IV (1250–1300 °C)

Products (the thinnest deposition layer, about 50 μm) were formed in zone IV. The length of this zone is about 8 mm. Large sheets with a width of about 10 μm across and thickness of several tens of nanometers have been identified using SEM as shown in Fig. 3(c). It can be seen that the nanosheets branch out at fixed angles and their endings are always triangular. This sheet-type structure has previously been observed for Ga_2O_3 and CdO.[2,19]

The results described above show that, by a simple chemical route involving H_2O in an Ar atmosphere, Al_2O_3 nanostructures with different morphologies and sizes were formed over a narrow temperature range between about 1100 and 1300 °C and a long deposition length of about 55 mm. All results suggest that the temperature in the reaction processes play a dominant role on the formation of the Al_2O_3 nanostructures.

The unique structure of the nanobelts and nanosheets strongly implies that their growth may be mainly determined by growth kinetics combined with thermodynamics. The vapor–liquid–solid (VLS) and vapor–solid (VS) crystal growth

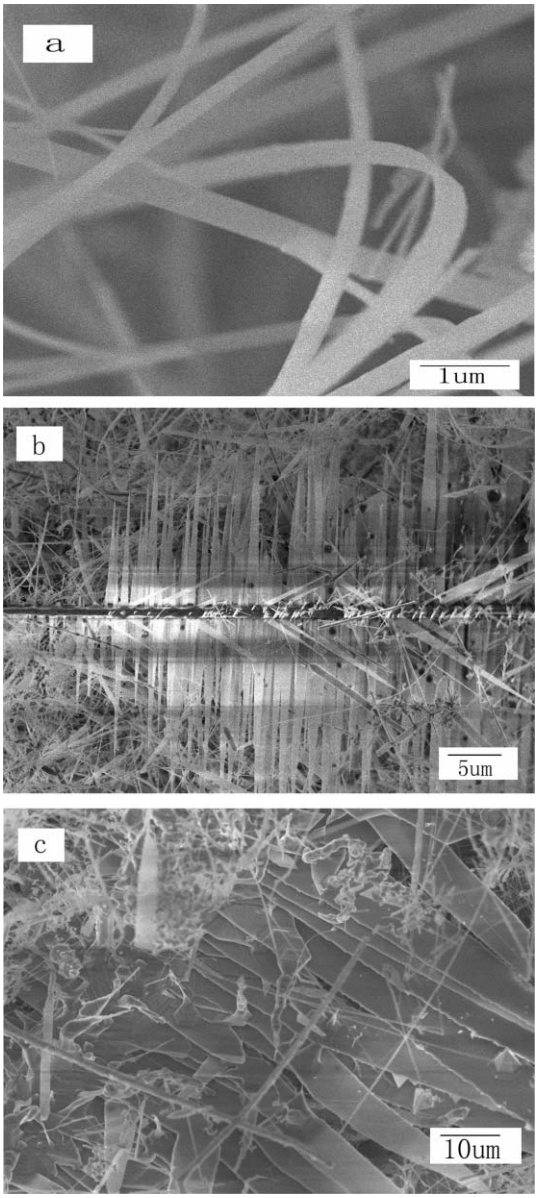

Fig. 3 SEM images showing the typical morphology of the as-synthesized Al_2O_3 nanostructures grown at (a) zone II, (b) zone III and (c) zone IV.

mechanisms have been widely used for the growth of one-dimensional nanostructures.[20–22] The VLS process was proposed for nanowires grown by a catalytically assisted technique, in which a nanoparticle is located at the growth front of the wire and acts as the catalytically active site for atom deposition. In the VS process, the oxide vapor, evaporated from the starting oxide at a higher temperature zone, directly deposits on a substrate at a lower temperature region and grows into belt-like nanostructures.[23] However, the chemical reactions involved and the detailed growth processes of the Al_2O_3 nanostructures here could be quite complicated. To understand the growth mechanism of these Al_2O_3 nanostructures, the following reaction should be considered:[19,24,25]

$$2\,Al + 3\,H_2O \rightarrow Al_2O_3 + 3\,H_2 \qquad (1)$$

The VS process might dominate the growth of these nanostructures since no nanoparticles have been observed at the tips of the Al_2O_3 nanostructures. The growth mechanism of Al_2O_3 nanobelts and nanosheets is similar to that of SnO_2 nanoribbons.[26] The morphologies of the Al_2O_3 nanobelts and nanosheets are determined by a combination of growth kinetics and thermodynamics. Thermodynamics requires the formation of crystals with well-faceted surface planes with low surface energy which is strengthened by kinetics where the growth rate is higher for high-energy surfaces and lower for low energy ones, and only surfaces with low energy could survive in the final crystals. However, as for the growth of low-dimensional nanostructures such as Al_2O_3 nanobelts and nanosheets, the difference in the growth rate for varied planes could be enhanced and a real thermodynamic equilibrium crystal shape would not be reached. This implies that the end surfaces of the nanoribbons may have a relatively higher surface energy than the top surfaces and the side surfaces, which may lead to a fastest growth rate normal to the end surfaces, medium growth rate for the side surfaces, and slowest growth for the top surfaces of the nanoribbons, forming a ribbon structure. The low-energy surface defines the planes that can present in the final product from the thermodynamic point of view, while the growth kinetics determinates the growth direction and the morphology of the product.

Although we have mainly discussed the effect of substrate temperature, other experiment parameters such as the gas flow rate, and the pressure in the furnace also have an influence on the nanostructure development. Both these parameters are correlated in a manner that higher flow rate increases the pressure. Additionally, higher temperature stimulates the faster evaporation of gas phase species and increase of the partial pressure of the reactants. All these parameters function cooperatively and lead to the final morphologies of nanoribbons and nanosheets. Here, the temperature is the determining factor for the morphology formation, a too high temperature leads to large crystals, while a too low temperature generally favor the formation of amorphous particles. The partial pressure of the reactants functions similarly to temperatures, namely, moderately high pressure promotes the formation of non-thermodynamic equilibrium nanoribbons and nanosheets, while a too high or too low pressure only leads to large particles or thermodynamic equilibrium shaped crystals. More work is underway to better understand the growth mechanism and to prepare nanostructures with different structures or different materials.

PL results taken from the products at the above four zones are shown in Fig. 4. PL measurements showed a blue luminescence band in the wavelength range of 400–500 nm with peak at 431 nm for zone I, 440 nm for zone II, 440 nm for zone III, and 440 nm for zone IV, respectively. It can be seen that the nanostructures with different sizes have almost the same PL band position; however, the intensity varies greatly from nanobelts to nanosheets. It was reported that heating

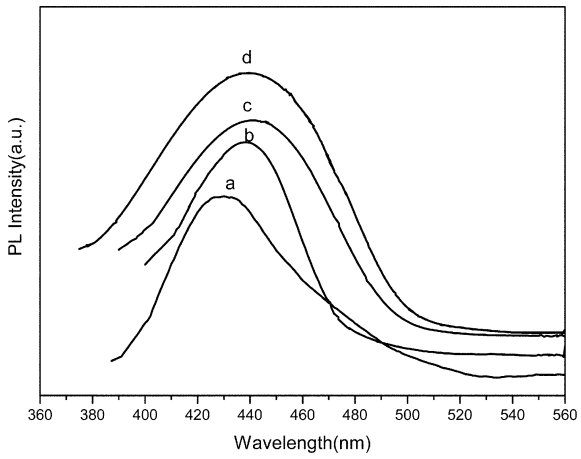

Fig. 4 PL spectra of the as-synthesized Al_2O_3 nanostructures formed at (a) zone I, (b) zone II, (c) zone III and (d) zone IV, respectively, measured with an excitation of the 255 nm line of a Xe lamp at room temperature.

Al_2O_3 under strongly reducing conditions resulted in the formation of oxygen vacancies.[27,28] Therefore, our Al_2O_3 nanostructures prepared under an oxygen deficient atmosphere could also contain many oxygen vacancies. In the present experiment, it can be seen that the intensity of the PL bands increased with the sizes of the Al_2O_3 nanostructures when the morphology changed from nanobelts to nanosheets (fig. 4). This result implies that the high specific surface area of the Al_2O_3 nanostructures should also favor the existence of oxygen vacancies.[29] On the basis of the PL results, we can also draw the conclusion that growth temperature correlates directly with the morphologies of the product, and is evidenced as the variation of the PL intensity with different product sizes. It has been reported that F^+ centers (oxygen vacancies with one electron) in α-Al_2O_3 cause ultraviolet or violet PL bands and blue PL bands in nanostructured alumina. For example, PL bands at 394 and 392 nm were observed from α-Al_2O_3 nanowires and nanobelts,[11] and two peaks in the wavelength region of 400–550 nm were observed from Al_2O_3 films.[30] We believe that the PL peaks observed in our experiment are intimately associated with the F^+ centers. Therefore, we proposed that the F^+ centers are most probably responsible for the PL emission from the Al_2O_3 nanostructures.

4. Conclusions

In summary, we have described a novel method for the synthesis of α-Al_2O_3 nanobelts and nanosheets by a simple chemical route, and the effect of substrate temperature on the growth of α-Al_2O_3 nanobelts and nanosheets has also been studied in detail by SEM. We believe that growth kinetics combined with thermodynamics is responsible for the formation of the nanobelts and nanosheets. PL measurements showed a strong blue luminescence band in the wavelength range of 400–500 nm, which could be attributed to the F^+ centers in the α-Al_2O_3 nanostructures. These α-Al_2O_3 nanostructures may possibly be useful as reinforcements in composites. In addition, considering their high specific surface area, optical properties, and low cost, these α-Al_2O_3 nanostructures are also suitable building blocks for use as protective films in composites.

Acknowledgements

We are grateful to National Major Project of Fundamental Research: Nanomaterials and Nanostructures (Grant No. 19994506) and the Natural Science Foundation of China (Grant No. 10074064) for the support of this work.

References

1 J. T. Hu, T. W. Odom and C. M. Lieber, *Acc. Chem. Res.*, 1999, **32**, 435.
2 Z. W. Pan, Z. R. Dai and Z. L. Wang, *Science*, 2001, **291**, 1947.
3 C. H. Liang, G. W. Meng, G. Z. Wang, Y. W. Wang, L. D. Zhang and S. Y. Zhang, *Appl. Phys. Lett.*, 2001, **78**, 3032.
4 Z. G. Bai, D. P. Yu, H. Z. Zhang, Y. Ding, X. Z. Gai, Q. L. Hang, G. C. Xiong and S. Q. Feng, *Chem. Phys. Lett.*, 1999, **303**, 311.
5 X. S. Peng, G. W. Meng, J. Zhang, X. F. Wang, Y. W. Wang, C. Z. Wang and L. D. Zhang, *J. Mater. Chem.*, 2002, **12**, 1602.
6 Y. C. Wang and I. C. Leu, *J. Mater. Chem.*, 2002, **12**, 2439.
7 Y. W. Wang, C. H. Liang, G. W. Meng, X. S. Peng and L. D. Zhang, *J. Mater. Chem.*, 2002, **12**, 651.
8 M. H. Huang, Y. Y. Wu, H. N. Feick, N. Tran, E. Weber and P. D. Yang, *Adv. Mater.*, 2001, **13**, 113.
9 V. Valcárcel, A. Pérez, M. Cyrklaff and F. Guitián, *Adv. Mater.*, 1998, **10**, 1370.
10 C. C. Tang, S. S. Fan, P. Li Chapelle, Lamy de la M and H. Y. Dang, *J. Cryst. Growth*, 2001, **224**, 117.
11 X. S. Peng, L. D. Zhang, G. W. Meng, X. F. Wang, Y. W. Wang, C. Z. Wang and G. S. Wu, *J. Phys. Chem. B*, 2002, **106**, 11163.
12 Z. W. Pan, Z. R. Dai, L. Xu, S. T. Lee and Z. L. Wang, *J. Phys. Chem. B*, 2001, **105**, 2507.
13 H. Y. Peng, Z. W. Pan, L. Xu, X. H. Fan, N. Wang, C. S. Lee and S. T. Lee, *Adv. Mater.*, 2001, **13**, 317.
14 C. H. Ye, G. W. Meng, Y. H. Wang, Z. Jiang and L. D. Zhang, *J. Phys. Chem. B*, 2002, **106**, 10338.
15 J. S. Lee, K. Park, M. Kang, I. Park, S. Kim, W. K. Cho, H. S. Han and S. Kim, *J. Cryst. Growth*, 2003, **254**, 423.
16 C. C. Chen, C. C. Yeh, C. H. Chen, M. Y. Yu, H. L. Liu, J. J. Wu, K. H. Chen, L. C. Chen, J. Y. Peng and Y. F. Chen, *J. Am. Chem. Soc.*, 2001, **123**, 2791.
17 JCPDS: 10-173.
18 N. W. Chen, D. W. Readey and J. J. Moore, *Ceram. Eng. Sci. Proc.*, 1994, **15**, 170.
19 L. Dai, X. L. Chen, X. N. Zhang, A. Z. Jin, T. Zhou, B. Q. Hu and Z. Zhang, *J. Appl. Phys.*, 2002, **92**, 1062.
20 R. S. Wagner and W. C. Ellis, *Appl. Phys. Lett.*, 1964, **4**, 89.
21 X. F. Duan and C. M. Lieber, *J. Am. Chem. Soc.*, 2000, **122**, 188.
22 S. S. Brenner and G. W. Sears, *Acta Metall.*, 1956, **4**, 268.
23 Z. R. Dai, Z. W. Pan and Z. L. Wang, *J. Phys. Chem. B*, 2002, **106**, 902.
24 B. Zheng, Y. Y. Wu, P. D. Yang and J. Liu, *Adv. Mater.*, 2002, **14**, 122.
25 L. Dai, X. L. Chen, W. J. Wang, T. Zhou and B. Q. Hu, *J. Phys.: Condens. Matter*, 2003, **15**, 2221.
26 Z. R. Dai, Z. W. Pan and Z. L. Wang, *Solid State Commun.*, 2001, **118**, 351.
27 K. H. Lee and J. H. Crawford, *Appl. Phys. Lett.*, 1978, **33**, 273.
28 K. H. Lee and J. H. Crawford, *Phys. Rev. B*, 1979, **19**, 3217.
29 C. H. Liang, G. W. Meng, Y. Lei, F. Phillipp and L. D. Zhang, *Adv. Mater.*, 2001, **13**, 1330.
30 Y. Zhu and P. P. Ong, *J. Phys.: Condens. Matter*, 2001, **13**, 4075.